Robotics and Computer-Integrated Manufacturing 38 (2016) 31–41

Contents lists available at ScienceDirect

Robotics and Computer-Integrated Manufacturing

journal homepage: www.elsevier.com/locate/rcim

An engineering method for the power flow assessment in servo-actuated automated machinery: Mechatronic modeling and experimental evaluation

Enrico Oliva [a], Giovanni Berselli [b,*], Marcello Pellicciari [a], Angelo O. Andrisano [a]

[a] DIEF - Department of Engineering "Enzo Ferrari", University of Modena and Reggio Emilia, Italy
[b] DIME - Department of Mechanics, Energetics, Management and Transportation, University of Genova, Italy

ARTICLE INFO

Article history:
Received 19 November 2014
Received in revised form
18 September 2015
Accepted 19 September 2015
Available online 23 October 2015

Keywords:
Power flow assessment
Servo-actuated mechanism
Virtual prototyping
Design of Experiments

ABSTRACT

In this paper, an engineering method for the power flow assessment of a position-controlled servo-mechanism is outlined. The considered system is composed of a permanent magnet synchronous motor coupled to a standard power converter, and directly connected to a slider crank mechanism. After the accurate description of a consistent power flow model, a sequential identification technique is discussed, which allows to determine the dynamic parameters of linkage, electric motor and electronic driver by means of non-invasive experimental measures. The proposed model allows to accurately predict the major sources of power loss within the system.

1. Introduction

During the last few decades, a growing sensitivity on energy consumption and the related environmental issues has increased, leading to the conception of several Green Manufacturing techniques [1]. In particular, a special attention has been recently devoted to the development of novel methods and tools for the energy-optimal design of position-controlled servo-actuated mechanisms [2,3]. These energy saving methods usually rely on predictive models of the system power flow, whose accurate assessment requires a precise description of linkage, electric motor and electronic driver dynamics.

On the other hand, even though several servo-mechanism models may be easily found in the literature [4], the numerical parameters describing the system behavior are usually either unknown, rather inaccurate or covered by confidentiality agreements. For instance, the torque constant of the electric motors, together with the motor nominal efficiency, can be found in the component data-sheets. However, these data are often very roughly defined and useful only for approximate predictions. Similarly, the linkage parameters (such as nominal dimensions, masses and moments of inertia) can be determined by means of a generic CAD software only if a virtual prototype of the mechanical hardware is available and no third party equipment is employed. Therefore, proper identification techniques may become the only way to build reliable power models and to quickly evaluate a set of consistent model parameters.

Concerning these identification techniques, several approaches have been presented in the past literature, which are well addressed in multiple books [5] and surveys [6]. In general, a standard identification procedure consists of *modeling*, *Design Of Experiments* (*DOE*), *data acquisition* and subsequent *signal processing*, *parameter estimation*, *model validation*.

As for the modeling part, the generation of a system model is the first step of any identification technique. On one hand, the inclusion of all the physical phenomena that determine the dynamic behavior of the system allows to reduce potential systematic errors (i.e. bias errors [7]). On the other hand, complex models necessarily imply an increased number of parameters that need to be identified and, consequently, increased uncertainty of the identification results. Therefore, for a given application and accuracy requirement, the model complexity should be calibrated so as to minimize the unknown parameters as much as possible. For instance, in the field of industrial robotics, the parameter identification concerning the mechanical properties of serial

Abbreviation: PF, power flow; DOE, Design Of Experiments; DM, dynamic model; LP, Linear in Parameters; RMSE, Root Mean Square Error; NRMSE, Normalized Root Mean Square Error

* Corresponding author. Department of Mechanics, Energetics, Management and Transportation, University of Genova, Italy.
E-mail addresses: enrico.oliva@unimore.it (E. Oliva), giovanni.berselli@unige.it (G. Berselli), marcello.pellicciari@unimore.it (M. Pellicciari), angelooreste.andrisano@unimore.it (A.O. Andrisano).

http://dx.doi.org/10.1016/j.rcim.2015.09.013
0736-5845/

Nomenclature

q, $\dot{q}$, $\ddot{q}$ motor position, velocity and acceleration
τ_{mot}, τ_{rb}, τ_{pay} motor torque, inertial torque due to the mechanism rigid bodies behavior, inertial torque due to the payload effect
$\tau_{f,cr}$, $\tau_{f,sl}$, $F_{f,sl}$ crank and slider friction torques, slider friction force
i_{mot}, i_{pay}, i_{inv}, v_{inv} motor current, motor current rate due to the payload effect, inverter current and inverter voltage (see Fig. 1)
L_{mot}, L_{inv} motor and inverter electrical losses
P_{mech}, P_{inv} mechanical and inverter powers (see Fig. 1)
$\dot{q}_{max}$, $\ddot{q}_{max}$ maximum motor velocity and acceleration
ω_f, N_h, q_0, a_{iota}, b_ι fundamental frequency, no. of harmonics, position offset and coefficients of Fourier Series exciting trajectories
f_s, T_s sampling frequency and period
N_s, N_r no. of samplings during one trajectory and no. of repetitions for each trajectory
$\mathcal{U}$, $\mathcal{T}$ potential energy and kinetic energy
$y_{G,\iota}$, $z_{G,\iota}$, z_B ι-th body barycentric position in y and y directions, slider displacement
ω_ι ι-th body angular velocity
r, l crank and rod lengths (see Fig. 3)
d_{cr}, d_{rod} distances between joints and centers of mass (see Fig. 3)
ν_{cr}, μ_{cr}, ν_{sl}, μ_{sl} crank Columbian and viscous coefficients, slider Columbian and viscous coefficients
m_{cr}, m_{rod}, m_{sl}, m_{pay}, m_ι crank, rod, slider, payload, ι-th body masses
J_{cr}, J_{rod}, J_{iota} crank, rod, ι-th body barycentric inertias
K_t, $\hat{K}_t$ torque constant, estimated torque constant
K_{Fe}, K_{sw}, K_{Cu}, K_{off} iron, switching, copper and offset losses parameters
$\boldsymbol{\Phi}$, $\boldsymbol{W}$, $\boldsymbol{Y}$, $\boldsymbol{\theta}$ regression matrix, observation matrix, dependent variable and parameters vector
Y^e, Y^p experimental and predicted values of the generic dependent variable Y
$\hat{\theta}$ estimated value of the generic parameter θ
$\sigma_{\hat{\theta}}$, $\sigma_{\hat{\theta}_r}$ standard deviation and relative standard deviation of the generic estimated parameter $\hat{\theta}$
σ_x standard deviation of the noise on the generic measured variable x (see Table 2)
$f_{\tau,nl}$, f_{pay}, f_{pd} torque function in its non-LP formulation, payload torque function, power demand predictive function
$\boldsymbol{\Phi}_{\tau,l}$, $\boldsymbol{\Phi}_d$, $\boldsymbol{\Phi}_{ld}$, $\boldsymbol{\Phi}_{pf}$ torque regression matrix in its non-minimal LP formulation and related parameters, dynamic, loaded dynamic and power flow regression matrices
$\boldsymbol{\theta}_{\tau,l}$, $\boldsymbol{\theta}_d := \boldsymbol{\theta}_\tau K_t^{-1}$, $[\boldsymbol{\theta}_{ld}$, $\boldsymbol{\theta}_{pf}$ parameters concerning non-minimal LP, dynamic, loaded dynamic and power flow models
$\boldsymbol{W}_d$, $\boldsymbol{W}_{ld}$, $\boldsymbol{W}_{pf}$ dynamic, loaded dynamic and power flow observation matrices
$\boldsymbol{q} = [q_\kappa]^T$, $\dot{\boldsymbol{q}} = [\dot{q}_\kappa]^T$, $\ddot{\boldsymbol{q}} = [\ddot{q}_\kappa]^T$, $\boldsymbol{i}_{mot} = [i_{mot,\kappa}]^T$ arrays of position, velocity, acceleration, and motor current data at the discrete time instant t_κ
$\boldsymbol{q}^e$, $\dot{\boldsymbol{q}}^e$, $\ddot{\boldsymbol{q}}^e$, $\boldsymbol{i}^e_{mot}$, $\boldsymbol{P}^e_{inv}$, $\boldsymbol{P}^e_{mech}$ arrays of averaged experimental values for motor position, velocity, acceleration, current, inverter power, mechanical power
$\boldsymbol{i}^p$, $\boldsymbol{P}^p_{inv}$, $\boldsymbol{P}^p_{mech}$ arrays of predicted values for motor current, inverter power, mechanical power
x^e_κ, $x_{\iota,\kappa}$ average value of the generic variable x during the κ-th time instant, κ-th sample of the ι-th repeated experiment.

manipulators (i.e. the determination of links' masses and moments of inertia) is based on the use of a dynamic model which is linear with respect to the parameters to be identified [8,9]. These kinds of models will be referred to as Linear-in-Parameters (LP). This linearity property is extremely interesting as long as it considerably simplifies the parameter estimation phase, as discussed below. Similar LP models can also be applied in order to estimate some electric motor parameters, as shown in [10]. On the other hand, nonlinear dynamic effects such as mechanical friction, several actuator characteristics or the linkage dynamics when dealing with closed kinematic chains introduces challenges in the modeling phase which, in several cases, still require further research (as pointed out in [6]).

Regarding the DOE and the subsequent phases of data acquisition and signal processing, accurate identification procedures involve specifically designed experiments which are executed on a physical prototype. The available data (namely, the input value for the above-mentioned models) is then obtained through direct measures via a number of sensors and subsequently improved in terms of signal-to-noise ratio. Naturally, from a practical point of view, the number of sensors should be reduced to a minimum when possible. As highlighted in [7], the DOE phase is a subject that has received particular attention both in the statistical and robotic literature. For instance, focusing on robot identification, a set of joint trajectories is usually imposed, the related joint torques being subsequently measured. In this case, a number of DOE approaches exist, such as fifth-order polynomials interpolating between finite sets of joint positions/velocities [11] or finite sequences of joint accelerations [12].

Subsequently, the system parameters are computed during the estimation phase. In the class of estimation algorithms, three common methods employed in the past literature are the least squares method, the Kalman filtering and the maximum-likelihood estimation [7]. The least square method, applicable only when dealing with LP models, is a noniterative technique that determines the parameter estimates in a single step via singular value decomposition. Alternatively, the Kalman filtering algorithm is applicable also in case of nonlinear models, although it has been proven to be less effective for off-line identification [13,14]. Similarly, the maximum likelihood estimation provides consistent estimates with minimal uncertainty and is usually solved with iterative search routines, such as the Levenberg–Marquardt algorithm. The drawbacks of the maximum likelihood estimation are the necessity of an initial guess for the parameter estimates and the possibility to converge to a local minimum representing a suboptimal solution. As a last example, a new technique using real-coded genetic algorithms has been employed in [15], for application on a servo-controlled slider-crank mechanism. Results are compared to those obtained via the least square method, which proved to be superior in terms of computational times.

On the basis of the literature review it can be stated that:

- Well-established procedures have been previously employed for assessing the inertial parameters of serial manipulator [7,16,17] or simple linkages [15,18]. In parallel, similar techniques have been used for the determination of some electrical motor parameters [10,19,20]. Nonetheless, none of the above-mentioned literature considers the servo-controlled system as a whole, by combining the influence of mechanical dynamics, electric motor dynamics and inverter behavior.

- Several model of the Power Flow (PF) within servo-actuated machinery have been presented in the past, see e.g. [2,3,21–23], the focus being the PF prediction when the system parameters are known. Hence, none of these models was specifically conceived nor optimized for identification purposes, namely derived in a LP formulation.

Owing to the aforementioned considerations, the objective of the present paper is to outline a novel engineering method for the PF assessment in single degree-of-freedom linkage systems directly coupled to permanent magnet synchronous motors. For validation purposes, the method is hereafter applied and experimentally evaluated on a slider-crank servo-mechanism, which is taken as a reference case study. The proposed technique is specifically based on the sequential identification of the mechanism dynamics followed by an assessment of the electrical drive and motor influence on the system PF. First, the dynamic parameters and the torque constant are detected together in the presence of a known payload acting on the slider [9,24]. Second, the electric drive PF is considered, taking into account the major electrical losses. The identified parameters are finally merged into an overall PF predictive model, whose accuracy is evaluated by comparing predicted and actual power demand along a randomly chosen test trajectory.

Differently from previous literature, the proposed identification method is characterized by the following features:

- Both dynamic and PF models are derived in a LP formulation, thus allowing a straightforward DOE and the use of fast and efficient least square estimation techniques. Such LP formulation has been achieved resorting to appropriate simplifications, suitable parameters definitions, and a non-trivial modeling effort (described in the following sections).
- Mechanical and electrical parts are combined to create a comprehensive PF model. Usually, the mechanical and the electric motor dynamics are treated separately. In addition, in the present work, the dynamic behavior of the inverter is also included.
- Only position and current values (quadrature current) on the motor and monophasic measurements of voltage and current on the drive are necessary to complete the identification process. Hence, from a practical point of view, the acquisition phase can be carried out without a power meter nor three phase measurements.

The paper is organized as follows: Section 2 outlines the conceptual steps of the identification method; Sections 3 and 4 describe the modeling procedure and the Design of Experiment (DOE); Section 5 discusses data acquisition and signal processing; Section 6 discusses the estimation phase; Section 7 deals with the model validation, whereas the experimental results are shown in Section 8. Finally, Section 9 draws the concluding remarks. In addition, basic notations (along with a list of acronyms) are included in the Nomenclature section for clarity.

2. Identification method

Permanent magnet synchronous motors are today the de facto industry standard for position controlled servo-systems [25]. A conceptual scheme of the single-d.o.f. servo considered in this paper is shown in Fig. 1 and comprises a power converter (composed of rectifier, DC-link and servo-inverter), which drives an electrical motor connected to a slider-crank mechanism. The variables P_{inv} and P_{mech} respectively denote the total electrical power delivered to the inverter and the total mechanical power delivered to the motor shaft. In addition, Fig. 1 highlights the arrangement of the measurement devices, namely the motor encoder and the current and voltage sensor (indicated via red circles, V, A, and q respectively denoting a voltage, a current or an angular position measure).

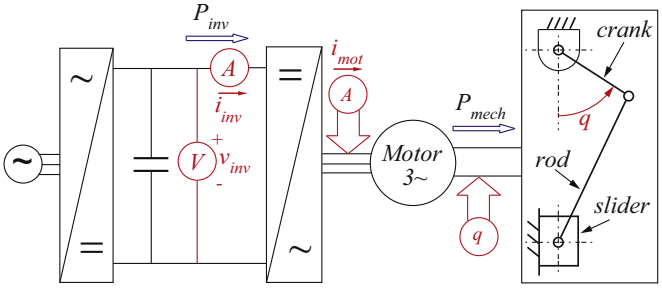

Fig. 1. Schematic of a simple servo-mechanism. Red circles indicate the sensors arrangement. (For interpretation of the references to color in this figure caption, the reader is referred to the web version of this paper.)

The whole identification process is summarized in the conceptual steps depicted in Fig. 2. The boxes represent the main phases of the procedure, wide arrows indicate the sequence of steps and thin arrows show the flux of information. Furthermore, quantities between blocks intuitively represent the outputs and the inputs of the previous and consecutive blocks respectively.

First, the dynamic model (DM) of the slider-crank is derived, assuming only the linkage geometric parameters as known. The DM describes the relation between the motor quadrature current, i_{mot}, and the motor angular position, q, velocity, $\dot{q}$, and acceleration, $\ddot{q}$ (hereafter referred to as *kinematic variables*). For identification purposes, the DM is excited using a suitable trajectory, defined during the DOE phase. The chosen motion is performed with and without a known payload attached to the slider, and the DM variables are sampled using the available measurement instruments (as depicted in Fig. 1). The requested set of de-noised variables, i.e. q, $\dot{q}$, $\ddot{q}$ and i_{mot}, is then obtained during the signal processing phase. The processed data are used to firstly assess the motor torque constant, K_t, whose estimated value is indicated as $\hat{K}_t$, along with the linkage dynamic parameters. As previously said, the estimation process can be faster and more accurate if the model to be identified is expressed in a LP formulation.

Before being accepted, the estimated DM is validated. Once the validation test has been accomplished, the identification of the power flows can begin. Initially, the effects on the PF of the identifiable electrical devices are modeled. The PF model describes the difference between the inverter power demand, P_{inv}, and the mechanical power, P_{mech}, as a LP function of kinematic variables and motor current. The PF exciting trajectory is chosen again by means of DOE, grounding on the knowledge of the already estimated dynamic parameters. The DM is exploited here to predict the motor current, allowing the definition of a DOE cost function which depends on the kinematic variables only. Then, the optimal exciting motion is performed and the sampled data are collected. The signal processing phase is subsequently carried out once more, defining the PF through inverter and electric motor. In this regard, it is important to know the torque constant, that is used to compute the mechanical power (note, indeed, that the processing phase of the PF model in Fig. 2 requires the estimated torque constant $\hat{K}_t$ as an input). At this point, the PF estimation and validation phases can be sequentially performed. Once all the models have been validated, their parameters can be used to define the predictive formulation of the power demand and to test the prediction accuracy.

3. Modeling

3.1. Mechanism dynamic model

As previously said, the mechanism DM aims at relating, in a LP

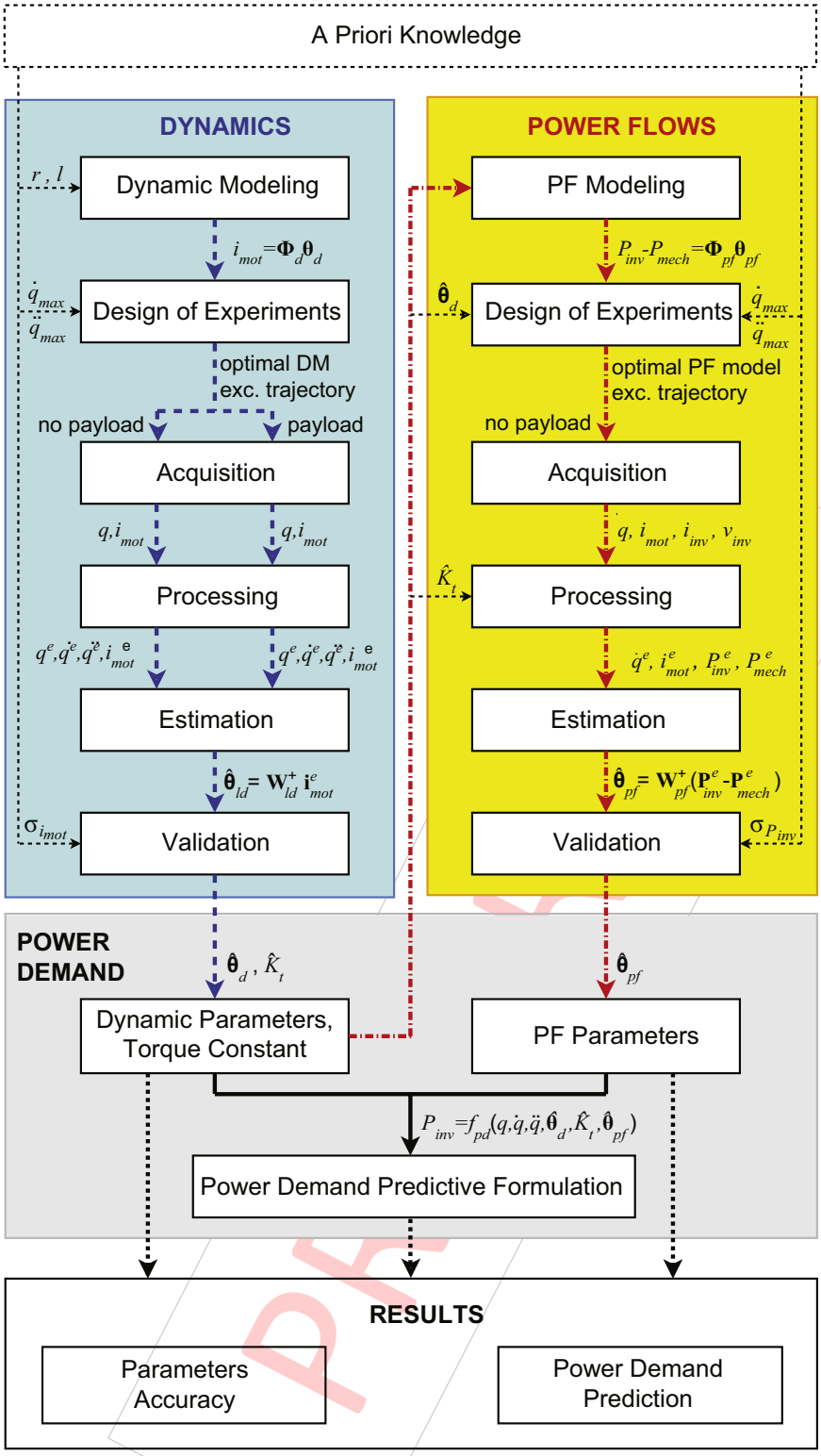

Fig. 2. Schematic representation of the employed identification method.

fashion, the motor current, i_{mot}, and the kinematic variables, q, $\dot{q}$, $\ddot{q}$. This LP expression is obtained considering only the essential physical phenomena contributing to the current flow. In particular, a formulation of the motor torque, τ_{mot}, is firstly derived by employing the Euler–Lagrange equation and the principle of virtual work [26], along with suitable friction models for the crank and slider kinematic pairs [27,28]. The friction torques on the passive rotational joints, namely crank-rod and rod-slider joints, are reasonably assumed as negligible. The derived model, that is non-LP, is then rephrased in a LP formulation by changing the parameters' definition. Unfortunately, some torque model parameters are redundant. Therefore, a minimal and identifiable set of parameters is defined by means of numerical techniques, as explained in [16, pp. 417–420]). Once the identifiable formulation of the motor torque is available, the DM can be finally derived considering motor torque and current as proportional [16, p. 299], the

torque constant K_t being the proportionality constant.

Motor torque derivation: The employed formulation of the motor torque takes into account the torque contributions $\tau_{f,cr}$, $\tau_{f,sl}$, and τ_{rb}, respectively due to crank friction, slider friction, and linkage inertia. Hence, the overall motor torque, τ_{mot}, can be written as

$$\tau_{mot} = \tau_{f,cr} + \tau_{f,sl} + \tau_{rb} \tag{1}$$

Crank friction torque, $\tau_{f,cr}$, directly acting on the motor shaft, and slider friction force, $F_{f,sl}$, acting on the slider moving surface, are modeled using the following basic and effective formulations:

$$\tau_{f,cr} = \nu_{cr}\,\mathrm{sign}(\dot{q}) + \mu_{cr}\dot{q} \tag{2}$$

$$F_{f,sl} = \nu_{sl}\,\mathrm{sign}(\dot{z}_B) + \mu_{sl}\dot{z}_B \tag{3}$$

where $\dot{z}_B$ is the slider velocity (z_B being the slider displacement), ν_{cr} and μ_{cr} are the crank Coulomb and viscous friction coefficients, whereas ν_{sl} and μ_{sl} are the slider Coulomb and viscous friction coefficients respectively. The input torque due to the slider friction is subsequently derived reducing $F_{f,sl}$ to the motor shaft by means of the virtual work principle, such that

$$\tau_{f,sl} = \frac{\partial z_B}{\partial q} F_{f,sl} \tag{4}$$

where z_B, as well as $\dot{z}_B$, are derived as a function of the kinematic variables, and of the crank and rod lengths, r and l, shown in Fig. 3 and assumed as known. Then, defining $\mathcal{T}$ and $\mathcal{U}$ as the mechanism kinetic and potential energies, the inertial term, τ_{rb}, is derived employing the Euler–Lagrange equation, such that

$$\tau_{rb} = \frac{d}{dt}\left(\frac{\partial(\mathcal{T}-\mathcal{U})}{\partial\dot{q}}\right) - \frac{\partial(\mathcal{T}-\mathcal{U})}{\partial q} \tag{5}$$

Kinetic and potential energies are simply derived as

$$\mathcal{T} = \sum_{\iota=1}^{3} \frac{1}{2} J_\iota \omega_\iota^2 + \frac{1}{2} m_\iota \left[\dot{y}_{G,\iota}^2 + \dot{z}_{G,\iota}^2\right] \tag{6}$$

$$\mathcal{U} = -\sum_{\iota=1}^{3} m_\iota g z_{G,\iota} \tag{7}$$

where, referring to the single ι-th rigid body, J_ι is the barycentric inertia, ω_ι is the angular velocity, m_ι is the mass, $z_{G,\iota}$ is the barycentric position in the z direction, $\dot{y}_{G,\iota}$ and $\dot{z}_{G,\iota}$ are the barycentric velocities in the y and z directions respectively, and g is the acceleration of gravity. It has to be noticed that the motor rotor is considered as rigidly connected to the crank, as long as a direct-drive servo-mechanism is considered (i.e. the absence of gear reducer). In particular, with reference to Fig. 3, let one respectively define d_{cr} and d_{rod} as the distances between crank and rod centers of masses and either point O or point A. All the positions and velocities exploited in Eqs. (6) and (7) are then symbolically derived as functions of the kinematic variables q and $\dot{q}$, of the known crank and rod lengths, r and l, and of the unknown distances, d_{cr} and d_{rod}. Hiding the dependence on the known constants r and l, and summing up the different contributions defined in Eqs. (2), (4) and (5), the motor torque, τ_{mot}, can be written as

$$\tau_{mot} = f_{\tau,nl}\left(q, \dot{q}, \ddot{q}, \boldsymbol{\theta}_{\tau,nl}^T\right) \quad \text{with} \tag{8}$$

$$\boldsymbol{\theta}_{\tau,l} = \left[J_{cr}, J_{rod}, m_{cr}, m_{rod}, m_{sl}, d_{cr}, d_{rod}, \nu_{cr}, \mu_{cr}, \nu_{sl}, \mu_{sl}\right]^T \tag{9}$$

where J_{cr} and J_{rod} are the crank and rod barycentric inertias,

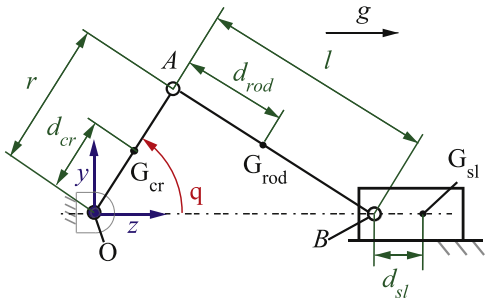

Fig. 3. Geometrical scheme of the slider-crank mechanism. The z-axis depicts the direction of gravity.

whereas m_{cr}, m_{rod}, m_{sl} are the crank, rod and slider masses respectively. Unfortunately, the model of Eq. (8) is not expressed in a LP formulation, since some of the rigid bodies' inertial parameters are multiplied by each other or raised to the second power.

Linear-in-Parameters formulation: It has been noticed that it is possible to rephrase model of Eq. (8) in a LP formulation by redefining $\boldsymbol{\theta}_{\tau,nl}$ in the following fashion:

$$\boldsymbol{\theta}_{\tau,l} = \left[J_{cr} + m_{cr}d_{cr}^2, J_{rod} + m_{rod}d_{rod}^2, m_{cr}d_{cr}, m_{rod}d_{rod}, m_{rod}, m_{sl}, \nu_{cr}, \mu_{cr}, \nu_{sl}, \mu_{sl}\right]^T \tag{10}$$

The following LP models for the motor torque is then obtained:

$$\tau_{mot} = \boldsymbol{\Phi}_{\tau,l}(q, \dot{q}, \ddot{q})\boldsymbol{\theta}_{\tau,l} \tag{11}$$

where $\boldsymbol{\Phi}_{\tau,l}$ is a regression row matrix which depends only on the kinematic variables. Unfortunately, as said, since some elements of the matrix $\boldsymbol{\Phi}_{\tau,l}$ are found to be linear dependent, the parameters defined in Eq. (10) are not fully identifiable using traditional system identification techniques. A suitable identifiable model, described using the minimum number of parameters, namely 8 parameters only, is derived employing numerical techniques based on QR factorization [16, pp. 417–420] and can be written as

$$\tau_{mot} = \boldsymbol{\Phi}_d(q, \dot{q}, \ddot{q})\boldsymbol{\theta}_\tau \tag{12}$$

where the vector of parameters $\boldsymbol{\theta}_\tau$ is defined as

$$\boldsymbol{\theta}_\tau = \begin{bmatrix} J_{cr} + m_{cr}d_{cr}^2 + m_{rod}r^2 + m_{sl}r^2 \\ J_{rod} + m_{rod}d_{rod}^2 + m_{sl}l^2 \\ m_{cr}d_{cr} + m_{rod}r + m_{sl}l \\ m_{rod}d_{rod} + m_{sl}l \\ \nu_{cr} \\ \mu_{cr} \\ \nu_{sl} \\ \mu_{sl} \end{bmatrix} \tag{13}$$

In addition, for $\iota = 1, \ldots, 8$, the single elements of the Regression row matrix $\boldsymbol{\Phi}_d = [\Phi_{d,\iota}]$ are shown in Table 1. Once the minimal LP formulation of τ_{mot} is derived, the DM is simply obtained imposing a linear motor torque–current relation, such that

$$\tau_{mot} = K_t i_{mot} \tag{14}$$

Substituting the torque model of Eq. (12) inside Eq. (14), the following formulation is achieved:

$$K_t i_{mot} = \boldsymbol{\Phi}_d(q, \dot{q}, \ddot{q})\boldsymbol{\theta}_\tau \tag{15}$$

Starting from Eq. (15), the DM is easily obtained as

$$i_{mot} = \boldsymbol{\Phi}_d(q, \dot{q}, \ddot{q})\left[\boldsymbol{\theta}_\tau / K_t\right] = \boldsymbol{\Phi}_d(q, \dot{q}, \ddot{q})\boldsymbol{\theta}_d \tag{16}$$

having defined, for the sake of simplicity, the dynamic parameters vector, $\boldsymbol{\theta}_d = \boldsymbol{\theta}_\tau K_t^{-1}$.

Table 1
Definition of the dynamic regression matrix elements.

Element	Definition
$\Phi_{d,1}$ (1/s^2)	$\ddot{q}$
$\Phi_{d,2}$ (1/s^2)	$\frac{c_q r^2(\ddot{q}c_q^3 r^2 + \ddot{q}c_q l^2 - \ddot{q}c_q r^2 - s_q \dot{q}^2 l^2 + s_q \dot{q}^2 r^2)}{h^4}$
$\Phi_{d,3}$ (m/s^2)	$s_q g$
$\Phi_{d,4}$ (m/s^2)	$\frac{r^2(-4\ddot{q}c_q^5 r^3 + 4c_q^4 s_q \dot{q}^2 r^3 - 4\ddot{q}hc_q^4 r^2 + 4hc_q^3 s_q \dot{q}^2 r^2 + 2gc_q^3 s_q r^2 - 4\ddot{q}c_q^3 l^2 r + 8\ddot{q}c_q^3 r^3 - 4\ddot{q}hc_q^2 l^2 + 4\ddot{q}hc_q^2 r^2)}{2h^3 l}$ + $\frac{r^2(4\ddot{q}c_q l^2 r - 4\ddot{q}c_q r^3 - 6s_q^3 \dot{q}^2 l^2 r + 6s_q^3 \dot{q}^2 r^3 + 4s_q \dot{q}^2 l^2 r - 4s_q \dot{q}^2 r^3 + 2s_{2q} h\dot{q}^2 l^2 - 2s_{2q} h\dot{q}^2 r^2 + s_{2q} g l^2 - s_{2q} g r^2)}{2h^3 l}$
$\Phi_{d,5}$ (1)	$\mathrm{sign}(\dot{q})$
$\Phi_{d,6}$ (1/s)	$\dot{q}$
$\Phi_{d,7}$ (m)	$\mathrm{sign}(\dot{q})\left\lvert rs_q[1 + \frac{rc_q}{h}]\right\rvert$
$\Phi_{d,8}$ (m^2/s)	$\dot{q}\{rs_q[1 + \frac{rc_q}{h}]\}^2$
Symbols:	$h = \sqrt{l^2 - r^2 \sin^2 q}$; $c_x = \cos x$; $s_x = \sin x$; x being a generic variable

3.2. Loaded dynamic model

The Loaded DM is simply an extension of the DM that also takes into account the influence of a known payload attached to the slider. The torque contribution due to the known payload mass, m_{pay}, is modeled considering the rate on the motor torque owing to the payload:

$$\tau_{pay} = \boldsymbol{\Phi}_d(q, \dot{q}, \ddot{q})\boldsymbol{\theta}_{pay} \tag{17}$$

where $\boldsymbol{\theta}_{pay}$ is derived from $\boldsymbol{\theta}_t$ from Eq. (13) by considering a slider mass equal to the payload mass and by neglecting all the other terms. The analytical description of $\boldsymbol{\theta}_{pay}$ is

$$\boldsymbol{\theta}_{pay} = [m_{pay}r^2, m_{pay}l^2, m_{pay}l, m_{pay}l, 0, 0, 0, 0]^T \tag{18}$$

By substituting Eq. (18) inside Eq. (17), the following formulation is derived:

$$\tau_{pay} = f_{pay}(q, \dot{q}, \ddot{q}, m_{pay}) \quad \text{with} \tag{19}$$

$$f_{pay} = m_{pay}(\Phi_{d,1}r^2 + \Phi_{d,2}l^2 + \Phi_{d,3}l + \Phi_{d,4}l) \tag{20}$$

The motor current rate due to the payload, i_{pay}, is then obtained simply dividing τ_{pay} by the torque constant K_t. Adding this contribution to the dynamic model of Eq. (16), the following equation is obtained:

$$i_{mot} = \boldsymbol{\Phi}_{ld}(q, \dot{q}, \ddot{q}, m_{pay})\boldsymbol{\theta}_{ld} \tag{21}$$

where $\boldsymbol{\Phi}_{ld}$ and $\boldsymbol{\theta}_{ld}$ are respectively the regression matrices and the parameters of the Loaded DM, defined as

$$\boldsymbol{\theta}_{ld} = \begin{bmatrix} \boldsymbol{\theta}_d \\ 1/K_t \end{bmatrix}$$

$$\boldsymbol{\Phi}_{ld}(q, \dot{q}, \ddot{q}, m_{pay}) = \left[\boldsymbol{\Phi}_d(q, \dot{q}, \ddot{q}), f_{pay}(q, \dot{q}, \ddot{q}, m_{pay})\right] \tag{22}$$

3.3. Power flow model

With reference to Fig. 1, the PF model of the servo-mechanism takes into account the power flowing to the inverter, P_{inv}, and the power flowing from the electric motor to the linkage mechanism, P_{mech}. Accurate and complex models of both motor and inverter have been widely investigated in the literature [4,19,10,20]. Nonetheless, in the identification method proposed in this paper only simple and effective formulations depending on the kinematic variables and on the motor quadrature current shall be used. Hence, the electric motor is modeled neglecting any energy storage and considering only the main physical contribution to the electrical losses. Similar to [2], these losses are described using the following model:

$$L_{mot} = K_{Cu}i_{mot}^2 + K_{Fe}\left\lvert\dot{q}\right\rvert \tag{23}$$

where K_{Cu} and K_{Fe} are the copper and iron losses parameters respectively. In parallel, the inverter model is obtained considering only the switching losses and neglecting again any energy storage:

$$L_{inv} = K_{sw}|i_{mot}| \tag{24}$$

K_{sw} being the switching losses parameter. According to experimental evidences, an offset term, K_{off}, is added to take into account any measurement offset or any constant loss term. Concerning these constant losses, as highlighted in [29], they are due to the permanent power requirements of the control electronics within the power converter. By summing up Eqs. (23) and (24) to this offset term, K_{off}, the PF model can be described in the following minimal LP fashion:

$$P_{inv} - P_{mech} = K_{Cu}i_{mot}^2 + K_{Fe}\left\lvert\dot{q}\right\rvert + K_{sw}\left\lvert i_{mot}\right\rvert + K_{off} \tag{25}$$

which can be rewritten in a matrix formulation as

$$P_{inv} - P_{mech} = \boldsymbol{\Phi}_{pf}(\dot{q}, i_{mot})\boldsymbol{\theta}_{pf} \tag{26}$$

where $\boldsymbol{\Phi}_{pf}$ is denoted as PF Regression Matrix, whereas the vector $\boldsymbol{\theta}_{pf}$ indicates the PF Parameters and is trivially defined as

$$\boldsymbol{\theta}_{pf} = \left[K_{Cu}, K_{Fe}, K_{sw}, K_{off}\right]^T \tag{27}$$

3.4. Predictive formulation of power demand

The symbolic formulation of the mechanical power, P_{mech}, is obtained by firstly multiplying the motor velocity by the motor torque, and then by exploiting the motor torque–current relation of Eq. (14):

$$P_{mech} = \dot{q}\tau_{mot} \rightarrow P_{mech} = \dot{q}K_t i_{mot} \tag{28}$$

The inverter power demand, P_{inv}, can be derived summing up the mechanical power of Eq. (28) and the PF model described by Eq. (26), such that

$$P_{inv} = \dot{q} K_t i_{mot} + \boldsymbol{\Phi}_{pf}(\dot{q}, i_{mot})\boldsymbol{\theta}_{pf} \tag{29}$$

Finally, by replacing the DM of Eq. (16) inside Eq. (29), the following predictive formulation is obtained:

$$P_{inv} = f_{pd}(q, \dot{q}, \ddot{q}, \boldsymbol{\theta}_d, K_t, \boldsymbol{\theta}_{pf}) \tag{30}$$

4. Design of Experiments

As said, in order to improve the convergence rate and the noise immunity during the estimation procedure, proper exciting experiments must be carefully selected. This DOE phase is thoroughly discussed in [5, Section 13], where the author treats the experiment design in a general context, showing how it can be performed for all types of models. However, in the case of LP models, the DOE can be formulated in a particularly straight-forward manner including three main steps: (a) the choice of a parameterization for the trajectory; (b) the selection of a cost function; (c) the derivation of the best exciting trajectory, by means of optimization techniques. Among all the possible methods to address these DOE steps, the particular choices made in the present work to optimally handle the considered case study can be described as follows:

- *Parameterization*: In order to obtain periodic and band-limited measurements, trajectories are parameterized as Finite Fourier Series:

$$q(t) = q_0 + \sum_{\iota=1}^{N_h} \left[a_\iota \sin(\iota \omega_f t) + b_\iota \cos(\iota \omega_f t) \right] \tag{31}$$

  where t represents time, q_0 is the position offset at $t=0$, ω_f is the fundamental frequency and N_h is the number of harmonics. Finding optimal values for a_ι and b_ι coefficients is now the DOE objective.
- *Cost functions*: Different cost functions can be chosen [16, pp. 296–298]. Considering the so-called observation matrix $\boldsymbol{W}$, where each row is defined as the evaluation of the regression matrix, $\boldsymbol{\Phi}$, at a discrete time instant, t_κ, the matrix condition number provides a good estimate of the parameters observability. For instance, optimal trajectory coefficients are characterized by a condition number of matrix $\boldsymbol{W}$ which is close to one. Thus, the cost function has been defined as

$$Cost = cond(\boldsymbol{W}) = \| \boldsymbol{W} \| \cdot \| \boldsymbol{W}^+ \| \tag{32}$$

  where the symbol $(\cdot)^+$ denotes the matrix Pseudo-inverse. In particular, the cost function for the DM exciting trajectory is

$$Cost_d = cond(\boldsymbol{W}_d(\boldsymbol{q}, \dot{\boldsymbol{q}}, \ddot{\boldsymbol{q}})) \tag{33}$$

  where, for $\iota = 1, \ldots, 8$ and $\kappa = 1, \ldots, N_s$, the vectors $\boldsymbol{q} = [q_\kappa]^T$, $\dot{\boldsymbol{q}} = [\dot{q}_\kappa]^T$, $\ddot{\boldsymbol{q}} = [\ddot{q}_\kappa]^T$ are arrays of length N_s, whose elements, q_κ, $\dot{q}_\kappa$, $\ddot{q}_\kappa$, are position, velocity and acceleration data derived from Eq. (31) at the discrete time instant t_κ. In parallel, the matrix $\boldsymbol{W}_d = [\Phi_{d,\iota}(q_\kappa, \dot{q}_\kappa, \ddot{q}_\kappa)]$ is computed accordingly on the basis of the Regression row matrix $\boldsymbol{\Phi}_d$ (see Eq. (12) and Table 1). Similarly, the cost function for the PF model exciting trajectory is defined as

$$Cost_{pf} = cond(\boldsymbol{W}_{pf}(\dot{\boldsymbol{q}}, \boldsymbol{i}_{mot})) \quad \text{with} \tag{34}$$

$$\boldsymbol{i}_{mot} = \boldsymbol{W}_d(\boldsymbol{q}, \dot{\boldsymbol{q}}, \ddot{\boldsymbol{q}})\hat{\theta}_d \tag{35}$$

  where $\hat{\boldsymbol{\theta}}_d$ are the estimated dynamic parameters, whereas, for $\iota = 1, \ldots, i$ and $\kappa = 1, \ldots, N_s$, the vector $\boldsymbol{i}_{mot} = [i_{mot,\kappa}]^T$ is an array of length N_s whose elements, $i_{mot,\kappa}$, are the motor currents sampled at the discrete time instant t_κ. In parallel, the matrix $\boldsymbol{W}_{pf} = [\Phi_{pf,\iota}(q_\kappa, \dot{q}_\kappa, \ddot{q}_\kappa)]$ is computed accordingly on the basis of the Regression row matrix $\boldsymbol{\Phi}_{pf}$ (see Eq. (26)).
- *Optimization*: The optimization step is carried out employing the *fmincon* Matlab function, which is used for constrained optimization problems and allows constraint enforcements on maximum velocities and accelerations, such as

$$|\dot{q}| < \dot{q}_{max} \quad \text{and} \quad |\ddot{q}| < \ddot{q}_{max} \tag{36}$$

  At the end of the procedure, optimal exciting trajectory coefficients, a_j and b_j, are found.

5. Data acquisition and signal processing

Naturally, the proposed method is widely dependent on the employed measuring instruments. In fact, factors like the accuracy of the measurements and the possibility to sample some variables rather than others determine the models that can be obtained. Due to the structure of the proposed method, the variables that are absolutely essential for identification purposes are the motor angular position, q, velocity, $\dot{q}$, and acceleration, $\ddot{q}$, the motor current, i_{mot}, and at least one power measure downstream of the motor. These variables can be directly sampled or derived during the processing phase. Therefore, the main aim of the data processing is to derive all the requested de-noised experimental variables. How this objective can be effectively achieved depends on the type of measures, e.g. mono-phase or three-phase electrical measures [30], and on the de-noising techniques that are applied, e.g. data filtering or averaging [5, Section 14].

For what concerns the present case study, as conceptually depicted in Fig. 1, the variables that are directly sampled are motor angular position, q, motor and inverter currents, i_{mot} and i_{inv}, and DC-link voltage, v_{inv}. Sampled angular positions are then filtered using a low-pass Butterworth filter in both forward and backward direction using the *filtfilt* Matlab function, thus removing noise without adding any phase shift to the signal [16, pp. 298–299]. Velocities, $\dot{q}$, and accelerations, $\ddot{q}$, are finally derived applying second order central differences to the filtered positions.

Subsequently, mechanical power, P_{mech}, and inverter power demand, P_{inv}, are computed as

$$P_{mech} = \dot{q}\hat{K}_t i_{mot} \tag{37}$$

$$P_{inv} = i_{inv} v_{inv} \tag{38}$$

where $\hat{K}_t$ is the estimated value of the torque constant, i_{inv}, v_{inv} and i_{mot} are measured variables, and $\dot{q}$ is derived from q as previously shown. Since an estimate for K_t is not initially known, the mechanical power can only be computed when the dynamic identification has been already performed, as shown in Fig. 2.

For what concerns signal de-noising, similar to [7], data averaging techniques over periodic trajectories have been employed. In this way, the signal-to-noise ratio is increased and the noise level of the signal is estimated. Denoting N_r as the number of repetitions of the same experiment and N_s as the number of samplings during each experiment, the employed formulas are

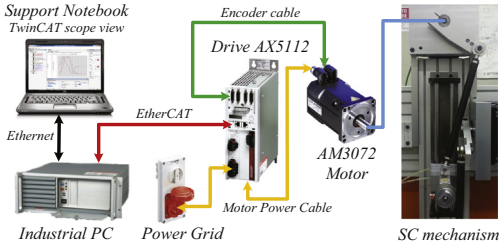

Fig. 4. Experimental setup.

$$x_\kappa^e = \frac{1}{N_r}\sum_{\iota=1}^{N_r} x_{\iota,\kappa} \quad \text{for } \kappa = 1, \ldots, N_s \tag{39}$$

$$\sigma_x^2 = \frac{1}{(N_r N_s - 1)}\sum_{\kappa=1}^{N_s}\sum_{\iota=1}^{N_r}\left(x_{\iota,\kappa} - x_\kappa^e\right)^2 \tag{40}$$

where x_κ^e is the average value of the generic variable x during the κ-th time instant, σ_x^2 is the sample variance of signal x, and $x_{\iota,\kappa}$ is the κ-th sample of the ι-th repeated experiment.

6. Estimation

Within the literature several estimation methods are shown [5, Section 7] which are applicable for generic model structures. However, when treating linear problems, it is well known that the least squares estimator has several advantages. In fact, the parameters derivation is computationally inexpensive and does not require to set any initial values. Since both the loaded DM

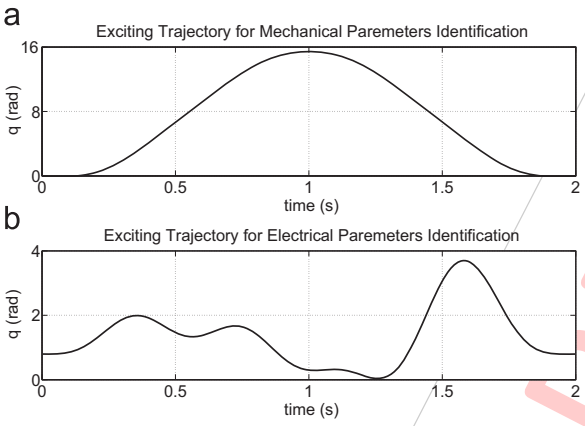

Fig. 5. Exciting trajectory for the (a) DM and (b) PF model respectively.

expressed by Eq. (21) and the PF model expressed by Eq. (26) are recast in a LP formulations, all the unknown parameters are identified using the least square estimator. In particular, the proposed method makes use of ordinary un-weighted least squares:

$$\hat{\boldsymbol{\theta}} = \left[\left(\mathbf{W}^T\mathbf{W}\right)^{-1}\mathbf{W}^T\right]\mathbf{Y} = \mathbf{W}^+\mathbf{Y} \tag{41}$$

where $\mathbf{Y} = [Y_\kappa]^T$ denotes a vector containing the generic dependent variable Y_κ evaluated at the discrete time instant t_κ.

Both dynamic parameters and torque constant are identified using the following formula:

$$\hat{\boldsymbol{\theta}}_{Id} = \left[\boldsymbol{W}_{Id}\left(\boldsymbol{q}^e, \dot{\boldsymbol{q}}^e, \ddot{\boldsymbol{q}}^e, \boldsymbol{m}_{pay}\right)\right]^+ \boldsymbol{i}_{mot}^e \tag{42}$$

where $\boldsymbol{q}^e$, $\dot{\boldsymbol{q}}^e$, $\ddot{\boldsymbol{q}}^e$ and $\boldsymbol{i}_{mot}^e$ are arrays of length $2N_s$ containing the averaged experimental values of q^e, $\dot{q}^e$, $\ddot{q}^e$ and i_{mot}^e in $2N_s$ sampling points. Recall, in fact, that the same exciting trajectory is repeated with and without a payload, m_{pay}, mounted on the slider. Hence, the payload mass vector, $\boldsymbol{m}_{pay}$, is an array of the same dimension of $\boldsymbol{q}^e$, whose values are either zeros when the payload is not mounted or m_{pay} when the payload is mounted.

Once the dynamic parameters and the torque constant are estimated, the PF parameters are identified using the following formulation:

$$\hat{\boldsymbol{\theta}}_{pf} = \left[\boldsymbol{W}_{pf}\left(\dot{\boldsymbol{q}}^e, \boldsymbol{i}_{mot}^e\right)\right]^+\left(\boldsymbol{P}_{inv}^e - \boldsymbol{P}_{mech}^e\right) \tag{43}$$

where $\dot{\boldsymbol{q}}^e$, $\boldsymbol{i}_{mot}^e$, $\boldsymbol{P}_{inv}^e$ and $\boldsymbol{P}_{mech}^e$ are arrays of averaged experimental values having length N_s. Indeed, during the estimation of the PF parameters, the exciting trajectories are repeated only without payload.

7. Validation

Before accepting the estimated models, it is a good practice to check their accuracy. If a certain model does not satisfy the validation phase, the previous phases (e.g. modeling, DOE and estimation) should be revised. Several validation techniques are known [5, Section 16], which may be applicable to generic model structures or to LP models only. In particular, when dealing with LP models, it is worthwhile to perform the analysis of the parameters accuracy. In fact, the confidence interval of the identified parameters can be derived by comparing the parameter values obtained over different exciting trajectories. However, this approach is very time consuming. Luckily, when dealing with LP models, the confidence interval can be quickly derived from the parameters

Table 2
Standard Deviation of the noise on the averaged measurements.

x	q (rad)	i_{mot} (A)	P_{inv} (W)
σ_x	1.30×10^{-3}	3.25×10^{-2}	6.65

Table 3
Identified parameter values and accuracy.

Parameter	Mean value	$\%\sigma_{\hat{\theta}_r}$
$\hat{\theta}_{d,1}$ (A s^2)	0.0175	0.31
$\hat{\theta}_{d,2}$ (A s^2)	0.0776	0.82
$\hat{\theta}_{d,3}$ (A s^2/m)	0.132	0.43
$\hat{\theta}_{d,4}$ (A s^2/m)	0.220	0.39
$\hat{\theta}_{d,5}$ (A)	0.0726	12.09
$\hat{\theta}_{d,6}$ (A s)	0.0150	3.11
$\hat{\theta}_{d,7}$ (A/m)	5.71	2.71
$\hat{\theta}_{d,8}$ (A s/m^2)	2.37	2.06
$1/\hat{K}_t$ (A/N m)	0.412	0.21
$\hat{K}_{Cu}$ (Ω)	1.03	2.22
$\hat{K}_{Fe}$ (W s)	0.581	2.78
$\hat{K}_{sw}$ (V)	5.67	2.80
$\hat{K}_{off}$ (W)	20.2	0.90

covariance matrix [5, App. II]. Once the Standard Deviation, $\sigma_{\hat{\theta}}$, of a certain parameter is derived, e.g. using the *lscov* Matlab function, its accuracy can be evaluated checking the Relative Standard Deviation, $\sigma_{\hat{\theta}_r}$, defined as

Table 4
RMSE and NRMSE of the predicted dependent variables over the validation trajectories.

Dynamic model validation trajectory		
	RMSE	NRMSE
i_{mot}	0.200 A	1.27%
Power flow model validation trajectory		
	RMSE	NRMSE
$P_{inv} - P_{mech}$	10.4 W	5.63%

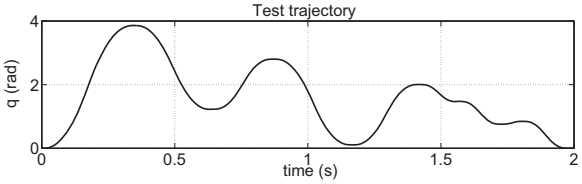

Fig. 6. Test trajectory.

Table 5
RMSE and NRMSE of the predicted inverter power demand over the test trajectory.

Test trajectory		
	RMSE	NRMSE
P_{inv}	8.96 W	1.57%

$$\sigma_{\hat{\theta}_r} = \frac{\sigma_{\hat{\theta}}}{\left|\hat{\theta}\right|} \tag{44}$$

In parallel to the parameter accuracy, it is surely worthwhile to estimate the residuals, i.e. the prediction error. This technique presents the considerable advantage of being suitable for all model structures and should be taken as a reference. In this case, the model predictive capability is tested on a validation trajectory that is consistently different from the ones used during the identification process. During this phase, the identified model is used to predict its output variable (namely i_{mot} for the DM and $P_{inv} - P_{mech}$ for the PF model) exploiting the experimental variables as inputs (namely q, $\dot{q}$, $\ddot{q}$ for the DM and $\dot{q}$, i_{mot} for the PF model). Denoting $\mathbf{Y}^p$ as the generic predicted output vector, the prediction accuracy of the model is derived comparing that vector with the experimental output vector $\mathbf{Y}^e$. In particular, the Root Mean Square Error (RMSE) and the Normalized Root Mean Square Error (NRMSE) can be used as representative values of the predictive accuracy:

$$RMSE = \| \mathbf{Y}^p - \mathbf{Y}^e \|_2 \tag{45}$$

$$NRMSE = \frac{\| \mathbf{Y}^p - \mathbf{Y}^e \|_2}{\max(\mathbf{Y}^e) - \min(\mathbf{Y}^e)} \tag{46}$$

Once both DM and PF models have been estimated and validated, the predictive equation of the inverter power demand can be defined and its accuracy checked analyzing its predictive capability on a random test trajectory. Employing Eqs. (16) and (26), the predictive outputs are computed as

$$\boldsymbol{i}_{mot}^p = \boldsymbol{W}_d(\boldsymbol{q}^e, \dot{\boldsymbol{q}}^e, \ddot{\boldsymbol{q}}^e)\hat{\boldsymbol{\theta}}_d \tag{47}$$

$$(\boldsymbol{P}_{inv} - \boldsymbol{P}_{mech})^p = \boldsymbol{W}_{pf}(\dot{\boldsymbol{q}}^e, \boldsymbol{i}_{mot}^e)\hat{\boldsymbol{\theta}}_{pf} \tag{48}$$

Finally, for what concerns the accuracy check on the power demand, the following expression is employed:

$$\boldsymbol{P}_{inv}^p = f_{pd}\left(\boldsymbol{q}^e, \dot{\boldsymbol{q}}^e, \ddot{\boldsymbol{q}}^e, \hat{\boldsymbol{\theta}}_d, \widehat{K_t}, \hat{\boldsymbol{\theta}}_{pf}\right) \tag{49}$$

where $\hat{\boldsymbol{\theta}}_d$, $\widehat{K_t}$, $\hat{\boldsymbol{\theta}}_{el}$ are the estimated parameters.

8. Experimental results

The proposed identification technique is validated employing experimental measures obtained on a servo-mechanism physical prototype, whose schematic is depicted in Fig. 4. The experimental rig is composed of a slider-crank mechanism directly coupled with a Beckhoff AM3072 synchronous motor and a Beckhoff AX5112 electrical drive. The control system is based on TwinCAT software, i.e. the PC-based control platform owned by Beckhoff, connected to the drive via EtherCAT fieldbus. The motor shaft angular positions, q, are measured using the motor encoder, whereas the electrical variables i_{mot}, i_{inv} and v_{inv} are provided by the proprietary software TwinCAT, with a sampling frequency f_s of 2000 Hz.

For what concerns the exciting trajectories, Fig. 5(a) and (b) respectively depict the optimal position profiles employed during DM and PF identification respectively. These optimal exciting motions have been parameterized as Finite Fourier Series (see Eq. (31)), the fundamental frequency ω_f being set to 1 rad/s and the number of harmonics N_h being set to 5 (following advices given in [7]). The Fourier Series' parameters have been computed in order to minimize cost functions of Eqs. (33) and (34) respectively, velocity and acceleration constraints of Eq. (36) being set as $\dot{q}_{max} = 25$ rad/s and $\ddot{q}_{max} = 250$ rad/s^2.

As for the signal processing results, Table 2 shows the Standard Deviation of the measured variables q and i_{mot}, and of the derived variable P_{inv}. These values are obtained as the square roots of the sample variances (see Eq. (40)) during a certain repeated trajectory.

For what concerns parameters accuracy, results are shown in

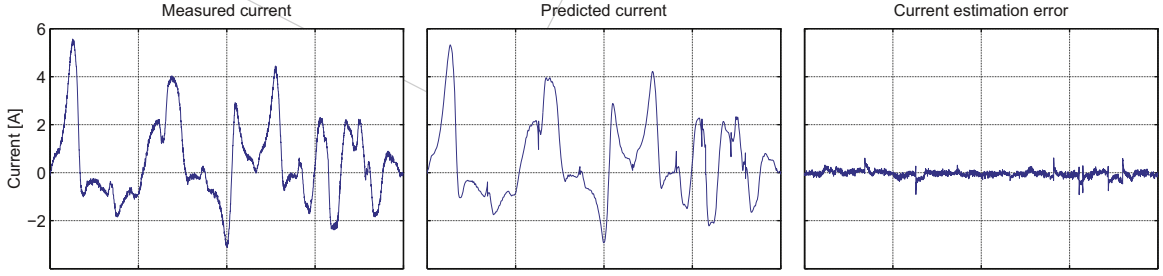

Fig. 7. Measured and predicted inverter current over the test trajectory.

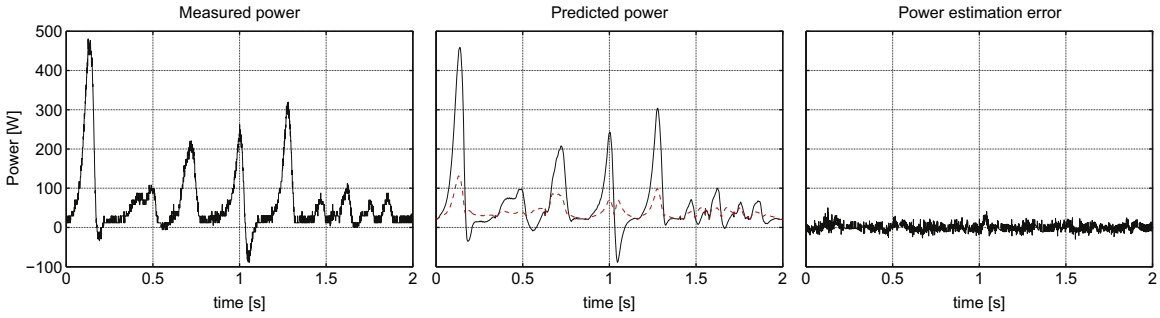

Fig. 8. Measured and predicted inverter power demand over the test trajectory. Red dashed line represents electric losses influence over the total predicted power demand. (For interpretation of the references to color in this figure caption, the reader is referred to the web version of this paper.)

Table 3, which confirms the effectiveness of the identification process. In particular, all parameters are characterized by $\%\sigma_{\hat{\theta}_r}$ lower than 3.11% (related to $\hat{\theta}_{d,6}$). The only parameter that has been estimated with a lower accuracy (namely $\%\sigma_{\hat{\theta}_r} = 12.09\%$) is $\hat{\theta}_{d,5}$, the one related to the Coulomb crank friction, probably because the simple friction model employed did not perfectly fit the friction behavior of the physical prototype. Subsequently, the estimated DM and PF models are validated on a random test trajectory, which is repeated only once and without any payload. As shown in Table 4, the NRMSE for the DM is slightly higher than 1%, showing an excellent predictive capability. In parallel, the RMSE for the PF model is lower than 11 W, showing an accuracy severely comparable with the one of the inverter power measurement itself (see Table 2).

Finally, the predictive formulation of Eq. (49), defined exploiting the parameters shown in Table 3, is used to predict the power demand over the test trajectory shown in Fig. 6, whose overall profile is chosen to be different from the one of the identification and validation trajectories. The trajectory consists in 9 acceleration trapezoidal motions, with jerk limitation, passing through 8 randomly chosen motor angles. Waiting time between different motions is set to zero. The experimental and predicted values are then compared using Eqs. (45) and (46). The results are numerically summarized in Table 5. In addition, Fig. 7 shows the value of the inverter current when the servo-mechanism is performing the test trajectory. The leftmost picture depicts the measured values, the central picture depicts the values predicted using the proposed model after parameter identification, whereas the rightmost picture depicts the prediction error, namely the difference between measured and predicted results. These graphs clearly highlight that the order of magnitude of the prediction error is comparable to the noise of the experimental measure. At last, Fig. 8 shows the value of the inverter power for the same test trajectory (the rightmost and central picture representing measured and predicted powers, the leftmost picture representing the prediction error). Also in this case, the graph shows an optimal prediction accuracy. Note that the central graph in Fig. 8 also depicts the influence of the power losses (red dashed line), numerically computed by means of the proposed model, highlighting the usefulness of the described technique to evaluate the system losses without the need to measure them directly.

9. Conclusions

A novel method for the power flow assessment of a position-controlled servo-mechanism has been discussed. At first, a power flow model of the system is proposed, describing the dynamic behavior of linkage, electric motor and inverter. Differently from previous literature, the model not only accounts for the major sources of power loss within the electronic driver, but it is also recast into a Linear-in-Parameters formulation to be optimally employed for identification purposes. The system parameters are indeed successfully identified via a set of non-invasive experimental measures, acquired while proper exciting trajectories are executed. Despite the simplifications necessarily introduced in the modeling part, the proposed formulation has shown excellent predictive capabilities, as long as the power prediction error is severely comparable to the noise of the power measure itself. At last, note that the proposed procedure can be easily re-arranged for assessing the power flow of generic single-degree-of-freedom linkage systems actuated via position-controlled electric motors.

Acknowledgments

The research leading to these results has received funding from the European Community's Seventh Framework Programme under Grant agreement no. 609391 (AREUS).

References

[1] E. Westkämper, The objectives of manufacturing development, in: Towards the Re-Industrialization of Europe, Springer, Stuttgart, Germany, 2014, pp. 23–37.
[2] C. Hansen, J. Oltjen, D. Meike, T. Ortmaier, Enhanced approach for energy-efficient trajectory generation of industrial robots, in: IEEE CASE, International Conference on Automation Science and Engineering, 2012, pp. 1–7.
[3] M. Pellicciari, G. Berselli, F. Balugani, On designing optimal trajectories for servo-actuated mechanisms: detailed virtual prototyping and experimental evaluation, IEEE/ASME Trans. Mechatron. 20 (5) (2015) 2039–2052.
[4] B.K. Bose, Modern Power Electronics and Ac Drives, Prentice Hall, Upper Saddle River, New Jersey, 2002.
[5] L. Ljung, System Identification: Theory for the User, second edition, Prentice Hall, Englewood Cliffs, New Jersey, 1999.
[6] J. Wu, J. Wang, Z. You, An overview of dynamic parameter identification of robots, Robotics Comput. Integr. Manuf. 26 (5) (2010) 414–419.
[7] J. Swevers, W. Verdonck, J. De Schutter, Dynamic model identification for industrial robots, IEEE Control Syst. 27 (2007) 58–71.
[8] C.G. Atkeson, C.H. An, J.M. Hollerbach, Estimation of inertial parameters of manipulator loads and links, Int. J. Robotics Res. 5 (3) (1986) 101–119.
[9] M. Gautier, S. Briot, New method for global identification of the joint drive gains of robots using a known inertial payload, in: IEEE CDC-ECC, Conference on Decision and Control and European Control Conference, 2011, pp. 1393–1398.
[10] M. Tenerz, Parameter estimation in a permanent magnet synchronous motor (Ph.D. thesis), Department of Electrical Engineering, Linköping, 2011.
[11] M. Gautier, W. Khalil, Exciting trajectories for the identification of base inertial parameters of robots, in: 30th IEEE Conference on Decision and Control, vol. 1, 1991, pp. 494–499.
[12] B. Armstrong, On finding 'exciting' trajectories for identification experiments involving systems with non-linear dynamics, in: IEEE International Conference on Robotics and Automation, vol. 4, 1987, pp. 1131–1139.
[13] M. Gautier, P. Poignet, Extended Kalman filtering and weighted least squares dynamic identification of robot, Control Eng. Pract. 9 (12) (2001) 1361–1372.
[14] P. Poignet, M. Gautier, Comparison of weighted least squares and extended Kalman filtering methods for dynamic identification of robots, in: IEEE International Conference on Robotics and Automation, vol. 4, 2000, pp. 3622–3627.
[15] J. Ha, R. Fung, K. Chen, S. Hsien, Dynamic modeling and identification of a

slider-crank mechanism, J. Sound Vib. 289 (2006) 1019–1044.
[16] W. Khalil, E. Dombre, Modeling, Identification and Control of Robots, Kogan Page Science, London, UK, 2004.
[17] E. Oliva, G. Berselli, F. Pini, Dynamic identification of industrial robots from low-sampled data, Appl. Mech. Mater. 328 (2013) 644–650.
[18] M. Huang, K. Chen, R. Fung, Comparison between mathematical modeling and experimental identification of a spatial slider-crank mechanism, Appl. Math. Model. 34 (2010) 2059–2073.
[19] N. Urasaki, T. Senjyu, K. Uezato, Influence of all losses on permanent magnet synchronous motor drives, in: IEEE IECON, 26th Annual Conference of the Industrial Electronics Society, 2000, pp. 1371–1376.
[20] P. Robet, M. Gautier, Decoupled identification of electrical and mechanical parameters of synchronous motor-driven chain with an efficient CLOE method, in: IEEE ICIEA, 8th International Conference on Industrial Electronics and Applications, 2013, pp. 1780–1785.
[21] M. Pellicciari, G. Berselli, F. Leali, A. Vergnano, A method for reducing the energy consumption of pick-and-place industrial robots, Mechatronics 23 (3) (2013) 326–334.
[22] V.A. Balogun, P.T. Mativenga, Modelling of direct energy requirements in mechanical machining processes, J. Clean. Prod. 41 (2013) 179–186.
[23] C. Hansen, J. Kotlarski, T. Ortmaier, Experimental validation of advanced minimum energy robot trajectory optimization, in: International Conference on Advanced Robotics, 2013, pp. 1–8.
[24] M. Gautier, S. Briot, New method for global identification of the joint drive gains of robots using a known payload mass, in: IEEE IROS, International Conference on Intelligent Robots and Systems, 2011, pp. 3728–3733.
[25] E. Kiel, Drive Solutions—Mechatronics for Production and Logistics, Springer, Berlin, Germany, 2008.
[26] B. Siciliano, L. Sciavicco, L. Villani, G. Oriolo, Robotics - Modeling, Planning and Control, Springer, Springer, London, UK, 2009.
[27] H. Olsson, K.J. Åström, C. Canudas de Wit, M. Gäfvert, P. Lischinsky, Friction models and friction compensation, Eur. J. Control 4 (1998) 176–195.
[28] P. Hamon, M. Gautier, P. Garrec, Dynamic identification of robots with a dry friction model depending on load and velocity, in: International Conference on Intelligent Robots and Systems (IROS), 2010, pp. 6187–6193.
[29] D. Meike, M. Pellicciari, G. Berselli, Energy efficient use of multirobot production lines in the automotive industry: detailed system modeling and optimization, IEEE Trans. Autom. Sci. Eng. 11 (3) (2014) 798–809.
[30] J.G. Webster, Electrical Measurement, Signal Processing, and Displays, CRC Press, Danvers, MA, 2003.